IOP Publishing Flex. Print. Electron. 7 (2022) 025006 https://doi.org/10.1088/2058-8585/ac6b6e

Flexible and Printed Electronics

OPEN ACCESS

RECEIVED
3 December 2021

REVISED
25 April 2022

ACCEPTED FOR PUBLICATION
28 April 2022

PUBLISHED
11 May 2022

PAPER

Routes towards manufacturing biodegradable electronics with polycaprolactone (PCL) via direct light writing and electroless plating

Mansour Abdulrhman[1], Adilet Zhakeyev[1], Carmen M Fernández-Posada[2], Ferry P W Melchels[3] and Jose Marques-Hueso[1,*]

[1] School of Engineering and Physical Sciences, Institute of Sensors, Signals and Systems, Heriot-Watt University, Edinburgh EH14 4AS, United Kingdom
[2] Maxwell Centre, Cavendish Laboratory: Department of Physics, University of Cambridge, JJ Thomson Avenue, Cambridge, CB3 0HE, United Kingdom
[3] School of Engineering and Physical Sciences, Institute of Biological Chemistry, Biophysics and Bioengineering, Heriot-Watt University, Edinburgh EH14 4AS, United Kingdom
[*] Author to whom any correspondence should be addressed.

E-mail: J.Marques@hw.ac.uk

Keywords: biodegradable, laser writing, electroless copper plating, selective metallization, polycaprolactone (PCL)

Abstract

The electronic industry has room for improvement in adopting cleaner strategies, both in production processes (often energy-intensive and polluting) and in waste management. Many small components like security tags are routinely disposed of via general waste, which could be reduced adopting biodegradable polymers. In this work, a method for selective deposition of metallic micro-tracks on polycaprolactone (PCL) for circuitry integration is presented. The polymer is biodegradable, flexible, suitable for 3D printing, and can be obtained from sustainable sources. Photoreduction of Ag ions was used to generate seeds for subsequent selective electroless copper (Cu) plating in a process that avoids common but undesirable compounds such as cyanides and palladium. Two different photopatterning methods were successfully used to achieve selective Cu plating: flood exposure with a 460 nm light-emitting diode (LED) and direct laser writing (DLW) using a 405 nm laser, achieving 47 ± 11 μm wide tracks. The deposition of uniform Cu layers on PCL substrates is demonstrated, with thicknesses of up to 14 μm and electrical conductivities of up to 2.06×10^7 S m^{-1}, which is near the conductivity of bulk Cu (5.89×10^7 S m^{-1}). Cu-plated interconnects were demonstrated to be fully functional for powering a 5 SMD LEDs circuit. Furthermore, DLW enabled the interconnect manufacturing on an uneven substrate. This method is flexible, selective, low-cost, vacuum-free and of minimized environmental impact, and it provides a new route towards the manufacturing of biodegradable electronics.

1. Introduction

New routes for substituting conventional electronics by biodegradable electronics will enable a reduction of e-waste in the near future. Since most electronic devices are made from non-decomposable materials, there is a growing interest in developing 'green electronics' by using biodegradable polymers [1–5]. These polymers are frequently derived from fossil fuel, although some of them can be bio-sourced from plants [6], adding the extra value of sustainability [7]. Biodegradable or transient electronics is finding possible applications for sensors [8], antennas [9], and transistors [10, 11], among others. Different biodegradable materials have been proposed for printed circuit board (PCB)s, such as plant-based residues [12] and combinations of cellulose and polylactic acid for PCB [13, 14], including multilayer configurations [15]. In this context, the first commercial products have started to appear [16]. Substrates constitute the majority of the volume and weight of an electronic device, therefore dictating the overall degradation behaviour of the device [2]. Small components, such as disposable sensors and electronic tags, are rarely recycled and would benefit from being biodegradable. Synthetic biodegradable polymers, such as

polycaprolactone (PCL), polylactide (PLA) and polyglycolide show a great deal of potential as substrates for electronic devices, due to the ester bond which imparts hydrolytic degradation [2, 17]. Moreover, biodegradable plastics such as PCL and PLA are cost effective to be produced [18, 19]. Among the biodegradable polymers, PCL is a semi-crystalline linear aliphatic polyester with a low melting point of 60 °C and tensile strength [20] of the order of 25 MPa which facilitates its processing, for instance via 3D printing [21–24]. PCL is a long-standing material, but at the right conditions it will fully degrade in 2–4 years [22]. This occurs through the breaking of the main molecular chain, triggered by different factors such as hydrolysis or oxidation [25]. Moreover, PCL can be produced from renewable sources. As a result, PCL presents itself as a cost-effective substrate for the fabrication of biodegradable electronic components. Efficient manufacturing of circuitry on biodegradable polymers such as PCL/PLA will encourage the industry to shift towards biodegradable electronics [26]. The metallization of plastics is popular due to several advantages, such as lightweight design flexibility and reduction of manufacturing costs. In recent years, several strategies were employed for the metallization of biodegradable polymers. For instance, demonstration the metallisation of electrospun PCL with Ag, via radio frequency magnetron sputtering [27]. Moreover, direct laser writing (DLW) technique to metallize 3D-printed substrates fabricated with PLA filament containing micro-sized Cu particles, using a conventional 1064 nm fibre laser to selectively remove the polymer and connect the Cu particles to each other [28]. A filament containing PLA mixed with graphene flakes was also used to 3D print patterns on substrates of pure PLA, which were then metallized via galvanic electrochemical deposition (electroplating) in a copper sulphate ($CuSO_4$) solution [29]. Electroless plating, a method which allows additive deposition of metals on non-conductive substrates, such as polymers and glass, offers a low-processing temperature as well as low cost compared to physical and chemical vapour deposition techniques [30–33]. The low temperatures involved in the electroless plating make it an ideal technique for the metallization of PCL. Conventionally, before the electroless metallization of polymers, modification of the surface layer was carried out via chemical [34, 35], plasma [36] and laser [37, 38] methods, followed by activation with metallization catalysts, which are usually metals from groups 8 and 11 of the periodic table, with palladium (Pd) being the most commonly used catalyst for surface activation [39]. For instance, $PdCl_2$ used for the surface activation of PLA substrates, followed by electroless Cu plating [36, 37, 40]. There is a variety of selective metallization methods for circuit structuring, such as photolithography [41], laser direct structuring (LDS) [42], laser direct imaging [43] and LISA (laser-induced selective activation) [44]. These conventional techniques are capital-intensive, with photolithography requiring a high number of steps, vacuum and clean-room conditions, whilst laser-based techniques, such as LDS and LISA, require expensive ArF excimer and Nd:YAG pulse lasers [36, 43, 45]. Selective metallisation of conductive micro-tracks on polyetherimide [46] and polyurethane elastomers [47] was successfully demonstrated using photo-reduced Ag nanoparticles (via photopatterning with 460 nm light-emitting diode (LED) light) as a seed layer for electroless Cu plating. Compared to nano-seeding catalysts based on Pd and other metals, photo-reduced Ag nanoparticles present an economic alternative and result in high-quality electroless Cu deposition [48]. It was also shown that the photoreduction rate of Ag can be enhanced through the use of potassium chloride (KCl) as photosensitizer [46, 48]. In this work, the direct selective metallization of biodegradable PCL substrates is presented, which involves surface treatment and electroless Cu plating. Specifically, the surface of PCL is activated with photosensitive (AgCl), via photopatterning using a blue light LED or a laser. Photo-reduced Ag ions subsequently provide a seeding layer for Cu ion adsorption during electroless plating. The conductivity of the resulting tracks is comparable to the conductivity of bulk Cu. Finally, this method was used to fabricate interconnects, which were proven to be fully functional in the electronic circuit powering a LED. In this work it is demonstrated the selective photopatterning of Cu tracks on biodegradable PCL substrates via electroless plating and laser writing, with potential for the fabrication of biodegradable electronics.

2. Materials and experimental details

2.1. Materials

All the reagents were used as received without further purification. (PCL M_n 80 000, fossil fuel sourced), isopropanol and copper sulphate ($CuSO_4$; 98%) were purchased from Sigma-Aldrich. Potassium hydroxide (KOH), silver nitrate ($AgNO_3$), potassium tartrate (99%), ammonia (NH_3; 18%) and sulfuric acid (H_2SO_4) were purchased from Fisher Scientific, UK. Sodium hydroxide (NaOH; 98.5%) and formaldehyde (37%) were purchased from Acros Organics.

2.2. PCL substrate treatment and photopatterning

The selective metallization of PCL was performed according to the processes outlined in figure 1. PCL samples of approximately 10–15 mm width and 300 μm thickness were used. The average surface roughness (Ra) was determined to be 45 $\pm$ 22 nm by profilometry. The samples were immersed in a 15 M KOH solution to undergo hydrolysis for 20 min at the temperature of 30°C. Following hydrolysis, the sample was rinsed with running deionized (D.I.)

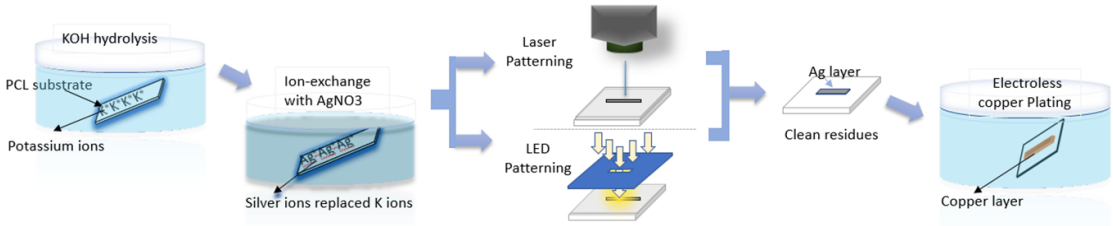

Figure 1. Overview of the process to deposit Cu track using light writing and electroless copper plating.

water for 2 min on each side. The hydrolysis aims to create hydroxyl groups (OHs) that silver ions can coordinate to. Next, the substrate was immersed in a 0.1 M $AgNO_3$ solution for 20 min at room temperature to perform ion exchange between potassium ions and Ag cations (Ag^+). Following ion exchange and a rinse with (D.I.) water, in order to accelerate the formation of the Ag nanoparticles (NP)s, the PCL sample was immersed in a 0.01 M KCl solution in ethanol: water (3:1) for 30 s at room temperature. KCl has been previously used to enhance the Ag photoreduction rate by replacing Ag ions with insoluble AgCl, which is photosensitive [46, 48]. This results in the rapid amalgamation of chloride and Ag ions in a well-known reaction, where the insoluble halide salt (AgCl) is precipitated on the PCL surface, as shown by equation (1):

$$Ag^+ + KCl \rightarrow K^+ + AgCl. \quad (1)$$

Light exposure with a LED or DLW triggers a photocatalytic transformation of AgCl into Ag NPs and chlorine gas, as shown by equation (2) [46]:

$$2AgCl\,(s) \rightarrow 2Ag\,(s) + Cl_2. \quad (2)$$

Selective photopatterning via flood exposure was performed using LED (Prizematix HUP-LED460) with a light output of 1 W, exposing each sample for a maximum of 30 s. A chromium on glass mask was used to selectively pattern PCL samples for 460 nm LED patterning. DLW was performed by using a computerised five-axis CNC machine, controlled by g-code, and equipped with a 405 nm laser diode (OFL-50-100-D, OdicForce Lasers, 32 μW and laser spot diameter about 30 μm). The removal of the residual unexposed AgCl from the PCL surface was performed by etching with a 18% NH_3 solution for 8 min, followed by immersion in 5% H_2SO_4 for 4 min and rinsing with DI water for 2 min after each cleaning step [49]. Besides the selectivity, this preparation of the seeding layer has the advantages of using silver rather than more expensive metals such as Pd and avoiding the use of toxic chromic acid or silver cyanide that other plating chemistries use, which results in a more environmentally friendly process.

2.3. Electroless plating of copper films on PCL

The solution for the electroless Cu bath was prepared using established procedure [48, 50, 51]. Briefly, 6 g of $CuSO_4$, 8 g of NaOH and 28 g of potassium tartrate were dissolved in 200 ml of DI water. Prior to the plating process, this solution was further diluted with DI water in the ratio of 1:1, followed by the addition of 1.5 ml of formaldehyde as a reducing agent. Photopatterned PCL samples were immersed into the electroless Cu bath for the specified time for each sample, with the solution kept at 30 °C. The formation of the Cu layer was observed after 10 min, with its thickness increasing with plating time.

2.4. Characterization

Fourier-transform infrared spectroscopy (FTIR) was performed using a Perkin-Elmer Spectrum 100 FTIR spectrometer in attenuated total reflection mode. X-ray photoelectron spectroscopy (XPS) analysis was carried out using an Escalab 250XI spectrometer (ThermoFisher Scientific, UK). The instrument was operated in constant analyser energy mode. A monochromatic Al-Kα source (1486.74 eV) and a flood gun for charge neutralization were used. Survey scans were acquired using pass energy of 100 eV, five scans were recorded using 0.5 eV steps and dwell of 50 ms, whilst for narrow scans, pass energy of 20 eV, step size of 0.05 eV and dwell time of 50 ms were used. The energetic position of the adventitious C1s emission line (binding energy of 284.6 eV) was chosen to calibrate the energy scale of XPS the spectra. Cu film thickness was measured by *KLA-Tencor's P-7* profilometer. To identify the average Cu thickness, six samples were prepared, and the average copper thicknesses with corresponding standard deviation was evaluated. The IPC-TM-650 scotch-tape test (3 M 600 scotch tape) was used to evaluate the adhesion quality of the plated Cu layers as a function of plating time. The tape came into contact with the whole surface of the sample (1 cm × 1 cm) and it was ensured that there was no air between the surface and the tape. After rapid pulling of the tape, the peeled residue on the tape was used to calculate the percentage of Cu that was removed, using ImageJ. The area of peeled copper was calculated and compared to the overall area of the sample. Optical images of the film surface were obtained using a Leica optical microscope. The conductivity of Cu

films was obtained by a four-point probe test using the kelvin four-wire technique (Keithley 2700 Multimeter) [52]. To obtain Cu conductivity for each sample, four samples were prepared, and the average Cu conductivity was calculated. The kelvin four-wire technique involves the pass of current (I) and the measurement of the resulting voltage (V) using four small pins which are in contact with the surface of the conductive film. Hence, four probes were attached to the sample to configure each probe location for forward and reverse current, and conductivity was calculated as reciprocal of the resistivity (ρ), which was calculated as shown in equation (3), where t is the Cu film thickness [53]:

$$\rho = \pi/\ln(2)\left(V/I\right)t = 4.532\left(V/I\right)t \quad (3)$$

$$\partial = 1/\rho. \quad (4)$$

Mechanical tests were performed to monitor the conductivity under bending and tensile stress. The bending test was done on a TA Instruments Q800 dynamic mechanical analysis (DMA) over 10 000 cycles. Every 1000 cycles, the resistance was measured five times by two-point probe. The tensile stress test was done on an Instron 5567 universal tensile tester, and the resistance was measured for each 1% strain increment.

3. Results and discussion

3.1. FTIR analysis

The FTIR spectrum of an untreated PCL sample exhibits the characteristic peaks of PCL, as shown in figure 2(a). The peaks in the 2990–2820 cm^{-1} region correspond to the CH_2 group asymmetric and symmetric axial deformations [54]. The strongest peak attributed to C=O stretching can be observed at 1721 cm^{-1} [55]. The intense and narrow peaks at 960 cm^{-1} and 940 cm^{-1} are attributed to the ester bond (C–O–C). The peak around 1166 cm^{-1} is due to the vibrations of C–O–C stretches, as reported in [56]. After hydrolysis, a broad OH peak appears in the 3600–3300 cm^{-1} region, which indicates the formation of hydroxyl end groups due to the cleavage of macromolecular chains caused by the hydrolysis [54]. The spectrum of the PCL sample that underwent K^+ ion exchange with Ag^+ ions, sensitization with KCl and photoreduction remains mostly unchanged compared to the only hydrolysed sample, except for the disappearance of the OH peak in the 3600–3300 cm^{-1} region, which can be attributed to the reduction occurrence of Ag ions, as AgCl can form Ag and Cl_2 by heating or illumination where complex reaction could occur in polymers after irradiation [57].

3.2. XPS analysis

Elemental composition analysis of the PCL surfaces was performed by XPS for each treatment step. XPS measurements of bare PCL's survey spectra show the presence of carbon and oxygen peaks at 284.6 eV and 532.04 eV respectively, which is the expected profile of the PCL chemical structure, shown in figure 3(a). The PCL sample that underwent hydrolysis with KOH shows a potassium peak at 292.7 eV, which reveals successful hydrolysis (figure 3(b)). The peak disappeared after the ion exchange step, given that the K is replaced by Ag. Following the sensitization with KCl, potassium peaks for chloride (K 2p) at 268 eV appeared, which could be attributed to KCl halide salt. This, coupled with the appearance of Ag peaks at 367.79 eV, confirms the successful exchange between K^+ and Ag^+ ions. After the photopatterning step, the chloride peaks disappeared, which would agree with the AgCl cleavage and photoreduction of Ag^+ ions into Ag^0 particles. In order to distinguish the elemental status of Ag^+ ions and photo reduced metallic Ag^0 on the surface of PCL, the Ag 3d region was analysed. Figure 3(c) shows that for the samples that underwent ion exchange, two peaks are present, which are attributed to Ag $3d_{5/2}$ and Ag $3d_{3/2}$. The sample treated with KCl exhibits a shift towards the lower binding energy of 367.97 eV (Ag $3d_{5/2}$), compared to the sample after the ion exchange step (368.73 eV). This may be assigned to the formation of Ag^+ ions in AgCl [58, 59]. The photopatterned sample exhibits an increase of the binding energy, corresponding to Ag $3d_{5/2}$ (368.64 eV), which is higher than 368.2 eV attributed to the Ag^0 of the metallic particles [60]. This suggests that the photo-reduced metallic Ag NPs have been oxidised, as the ones that are analysed are just on the surface of the material, since the binding energy value is in good agreement with the Ag $3d_{5/2}$ peak (368.6 eV) attributed to Ag^+ in Ag_2O [61]. Despite this oxidation, the silver content is sufficient for acting as a seeding layer for the electroless plating, as will be shown in next sections.

3.3. Effect of UV-Light exposure on the PCL surface

In order to test whether the UV exposure time degrades the sample surface, profilometer measurements were performed on samples after UV-LED exposure through a chromium mask (figure 4). After 4 min of exposure, visible lines of light-brown colour appeared, which indicates that silver NP have formed, as seen in figure 4(a). This exposure time is optimal for obtaining well-defined lines. After 6 min, the silver lines became darker, shown in figure 4(b), and they also broaden, given that light can be diffused in the plane. Increasing the time exposure to 10 min led to the complete darkening of the surface, which blurs the selective pattering, as shown

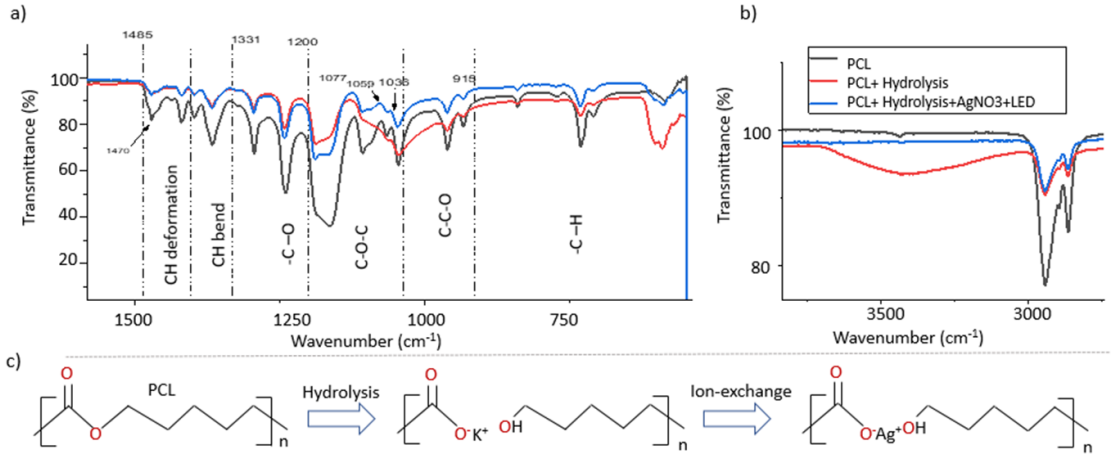

Figure 2. (a) FTIR analysis for PCL samples after hydrolysis and after $AgNO_3$ immersion and LED exposure. (b) OH stretch after the hydrolysis process and CH_2 asymmetric stretches. (c) PCL molecule after hydrolysis and ion-exchange.

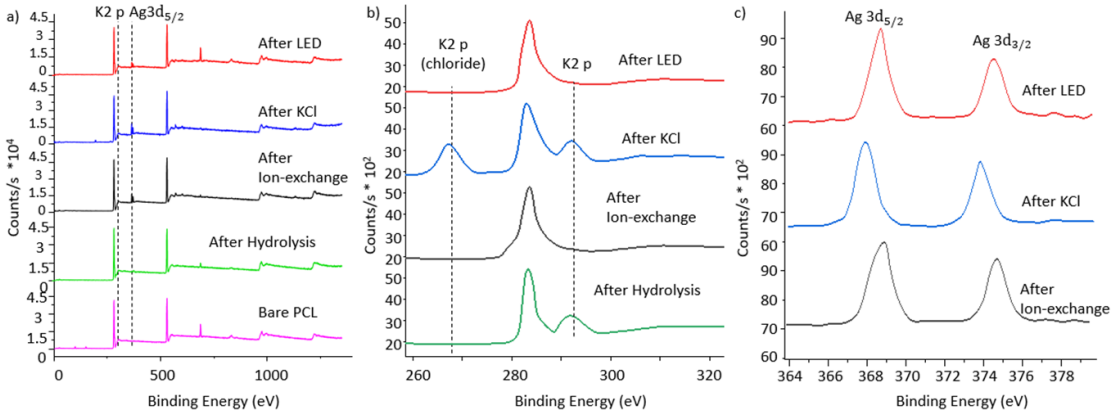

Figure 3. (a) XPS survey spectra of PCL samples after each step. (b) The K 2p peak appears after KCl treatment. (c) Narrow scan for position of the Ag 3d peaks indicate the state of the silver.

in figure 4(c). Profilometric measurements were performed on samples exposed at different times, as per figure 4(d). The profiles cover a distance of 180 μm and show oscillations in the range of 30–80 nm. This is indicative that the degradation should be smaller than 80 nm. Interestingly, the 4 min sample shows the largest oscillations, and the profiles are smoother for longer times. One hypothesis is that this could be due to the broadening of the lines and degradation happening even in the shaded areas. Because the following plating will produce Cu thicknesses of the order of microns, the possible degradation does not affect the final thickness.

Figure 4(e) shows a SEM image of a sample after the KCl treatment. The sample was encapsulated in resin before cleavage to obtain a cleaner cross-section. The treatment and silver content do not produce evident changes that can be identified easily. However, near the surface it is possible to appreciate bright particles. The Energy dispersive X-ray (EDX) analysis on one of these particles (figure 4(f)) reveals a composition where Ag (1.14% of atomic composition) and Cl (0.76%) are present. This could be due to the presence of AgCl and its partial reduction, which is consistent with the chemical interpretation of previous sections. The C (73.8%) and O (24.3%) would result from the background, since in EDX the signal is recorded for a 1 μm^2 region approximately.

3.4. Selective metallization: Cu thickness and conductivity

Figures 5(a)–(c) shows microscopic images of selectively metallized Cu patterns after LED flood exposure and the electroless copper plating, which were patterned using a chromium mask with 100 μm pitch size and different plating times. After plating for 8 min, the Cu layer is not completely developed. At longer plating times the Cu layer became increasingly better defined, with an optimum after 10 min. When the copper plating time was increased to 12 min, the Cu started to be deposited even on the unexposed surface of PCL, resulting in blurring of the Cu patterns. Figure 5(d) shows a Cu track fabricated by using the five-axis machine equipped with

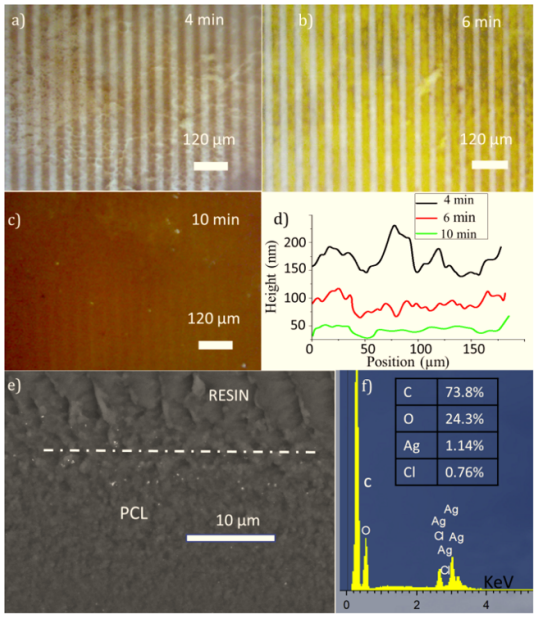

Figure 4. (a)–(c) UV-LED exposure for: (a) 4 min, (b) 6 min, (c) 10 min exposure. (d) Profilometric reading for different exposure times. (e) SEM of the PCL surface cross-section when embedded in resin. (f) EDX analysis on a bright particle, revealing some Ag and Cl content.

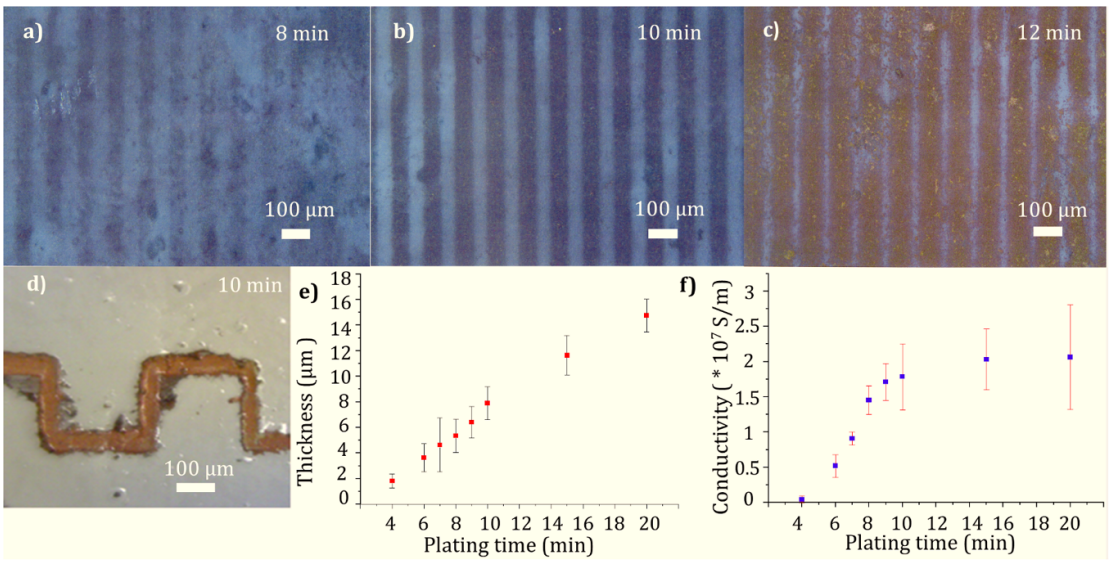

Figure 5. (a)–(c) Selective copper formation with LED flood exposure with chromium mask, (d) tracks by direct laser patterning after 10 min of plating time, (e) Effect of plating time on copper thickness. (f) Effect of plating time on electrical conductivity of deposited Cu layers.

the 405 nm laser. Patterning at 32 μW laser power produces reliable tracks without burning the PCL's surface. Electroless Cu plating was performed at the temperature of 30 °C for 10 min and resulted in uniform Cu tracks with average conductivity value of $(1.5 \pm 0.2) \times 10^7$ S m^{-1}. The Cu tracks fabricated by the DLW method exhibited high resolution, with average line widths of 48 μm.

Figure 5(e) illustrates the effect of the plating time on the thickness of Cu formed on the PCL substrates. After a first stage of nucleation, the Cu thickness gradually developed with increasing plating time, which agrees with the literature [47, 50, 62]. It starts to develop at about 4 min and results in uniform Cu layers after 6 min of plating. The largest Cu thickness of 14 μm was achieved after 20 min of plating time.

Figure 5(f) shows the effect of plating time on the conductivity of the deposited Cu layers. At low plating times, the deposited Cu layers exhibit brown colour and nonhomogeneous morphology with low electrical conductivity, derived from the roughness of the film [63, 64]. The conductivity increases with time, and starts to stabilize at 9 min,

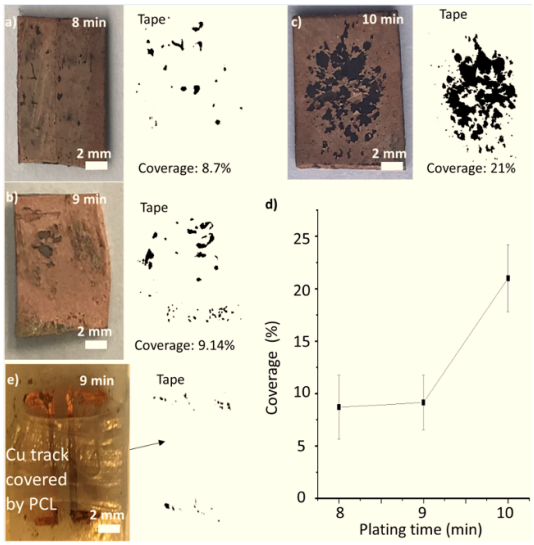

Figure 6. Evaluation of the adhesion between the plated copper layer and the PCL substrate at different plating times. The black colour indicates the removed copper from the surface of the metallized PCL. (a)–(c) Samples plated during different times (8, 9 and 10 min) showing different area coverage loss (8.7%, 9.14% and 21%, respectively. (d) Tracks covered by a PCL layer, acting as a protection cover for the Cu plated track. (f) Coverage as a function of plating time.

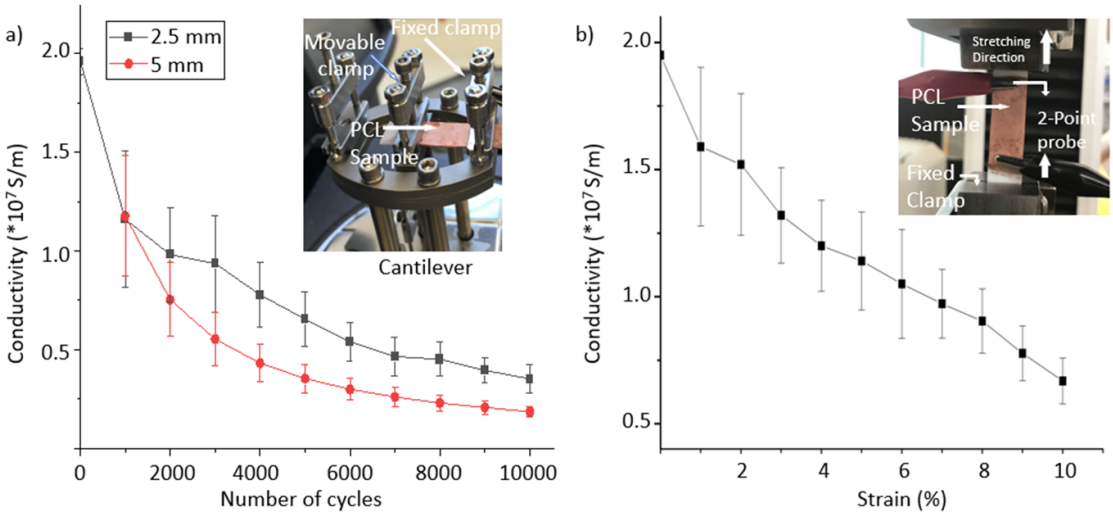

Figure 7. (a) Conductivity as a function of bending cycles. (b) Conductivity as a function of tensile stress.

with 1.71 $\times$ 10^7 S m^{-1}. The electrical conductivity reaches a plateau of around 2 $\times$ 10^7 S m^{-1}, with 2.06 $\times$ 10^7 S m^{-1} being the largest conductivity (20 min), which agrees with [47, 50, 62]. These values are common for electroless plated copper films and are comparable to the electrical conductivity of pure bulk Cu (5.89 $\times$ 10^7 S m^{-1}).

3.5. Adhesion test

The adhesion between the Cu layer and PCL substrate was evaluated using the tape test. While the adhesion is good for a nucleating film, when the thickness increases, new stress is built up in the film, resulting in poorer adhesion [65]. Figure 7 shows some relevant results of this effect. The plating time of 8 min results in the removal of approximately 9% of Cu, whilst after 10 min of plating, 21% of Cu is removed. This provides a narrow set of optimal parameters at around 8 min, where the film still shows sufficient adhesion while the conductivity is already high. Figure 6(d) shows the loss of coverage on the adhesion test correlated with plating time. In order to prevent the peeling of copper features, a PCL layer can be deposited on top as a protection cover, as can be seen in figure 6(e). This layer was placed by partially melting with a hot-air gun, which constitutes a simple packaging method.

3.6. Bending and tensile test

Figure 7(a) shows the electromechanical test of the copper film under bending cycles. A 35 $\times$ 11 mm^2 plated sample (9 μm Cu layer, and 300 μm thick

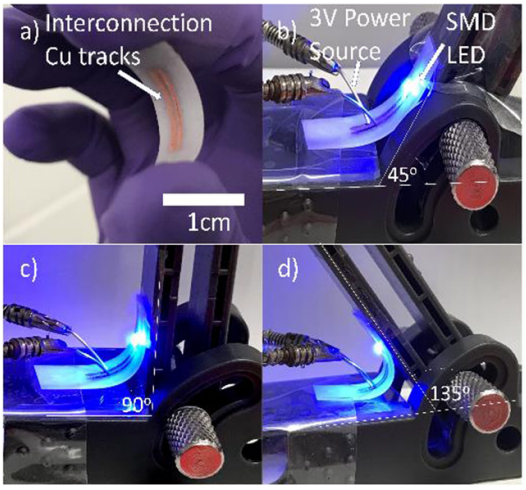

Figure 8. (a) Cu tracks fabricated on a 300 μm PCL substrate, and bending at three different angles: (b) 45°, (c) 90°, (d) 135°.

PCL substrate), is attached between a fixed clamp and a movable clamp, which applies strain at the central region with 1 Hz. Two different amplitudes for the movable clamp have been applied, 2.5 and 5 mm, corresponding to 1.6 and 2.5% strain, respectively. At zero bending, the conductivity of the copper film is 1.9×10^7 S m^{-1}. This conductivity is reduced with the number of bending cycles. After 1000 cycles the conductivity drops to 1.2×10^7 S m^{-1}, a loss of performance of 37%. At larger number of cycles, both samples show a different loss of performance, which is more severe for the sample suffering a higher strain. At 50 000 cycles, the conductivity is 0.65×10^7 S m^{-1} for 2.5 mm, which approximately doubles the 0.35×10^7 S m^{-1} of the 5 mm case. At 10 000 cycles, the conductivity is and 0.18×10^7 S m^{-1} for 5 mm amplitude and 0.35×10^7 S m^{-1} for 2.5 mm. Next, the electrical properties were measured under tensile stress, as seen in figure 7(b). The sample conductivity at zero strain is 1.85×10^7 S m^{-1}. This value decreases to 0.9×10^7 S m^{-1} at 8% strain, a 51% loss. This reduction is explained because the applied strain produces cracks and deformation of the Cu film. The test was finished at 10% strain which was the yield point of the PCL, with a final conductivity of 0.67×10^7 S m^{-1}, which is a 37% of the initial value before the test. Importantly, the mechanical properties of the Cu-coated PCL were in the normal range, with a Young's modulus of 308 $\pm$ 5 MPa (bending) or 300 $\pm$ 34 MPa (tensile) and a yield stress of 13.3 $\pm$ 2.5 MPa.

3.7. Flexible interconnection

Next, the capability of the technique to produce flexible interconnections was demonstrated. Figure 8(a) shows two laser-written Cu lines on a 300 μm PCL substrate to be used as an electrical connection. An SMD (surface-mount device) LED was soldered using silver paste (RSPro Rs 186-3600), and a 3 V power source closed the basic electrical circuit.

Gradual bending was performed for three different angles (45°, 90°, 135°), as shown in figures 8(a)–(c). There is no observable performance degradation under these bending conditions. When the bending increases and it is close to 180°, the light starts to flicker, which indicates that the operations region has been surpassed.

3.8. PCBs on PCL

To show the capability of the technique to print PCBs, different demonstrators were produced using laser writing patterning and electroless plating (figures 9(a) and (b)). Furthermore, an advantage of using laser writing is that the patterning can be done on 3D contours, uneven surfaces or cavities, which is a capability that most printing techniques lack. Figure 9(c) shows Cu tracks manufactured over a slit by laser writing. The substrate is a 2 mm thick PCL square, prepared by hot-embossing, with a slit 1.5 mm deep and 2 mm wide. The copper tracks are continuous all over the slit. Next, the capability of soldering multiple components and the performance of the circuits are shown in figures 9(d) and (e). The circuit of figure 9(e) was powered by a 3 V power supply and the LED was on for two weeks without any interruption or loss of performance. Soldering components using hot Sn would lead to thermal deformation. Hence, soft soldering using silver paste was used. A detail of the profile is shown in figure 9(f).

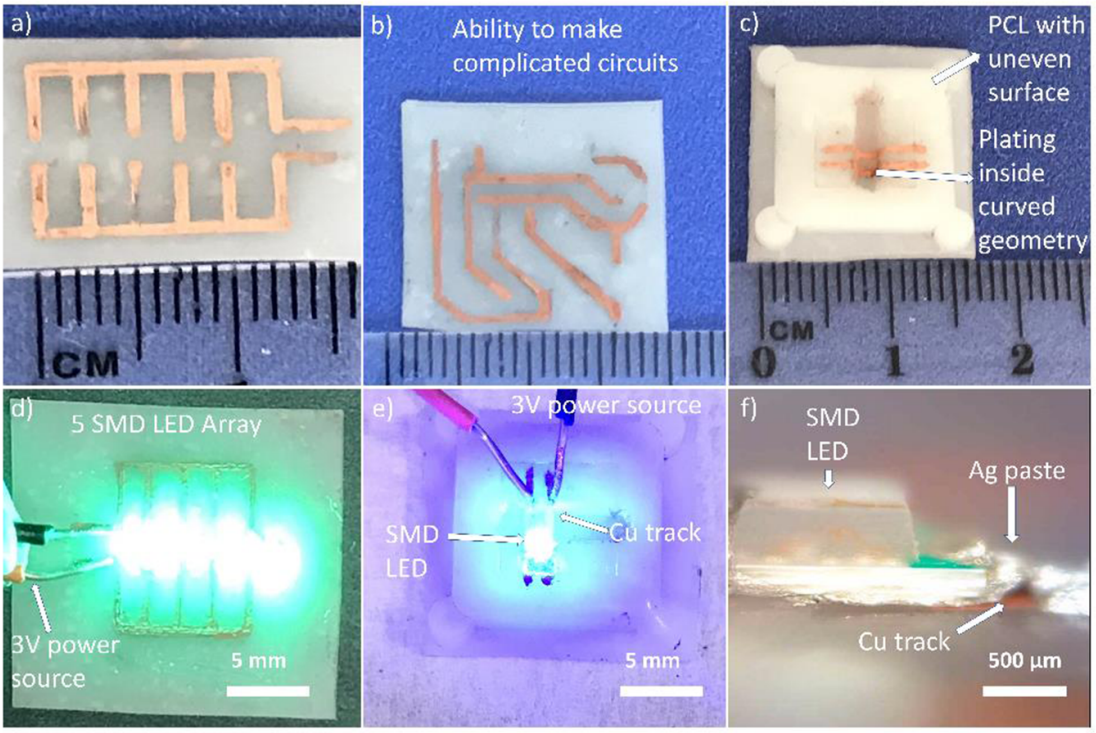

Figure 9. (a), (b) Laser-written and plated circuits on PCL substrates. (c) Plated tracks on uneven surface. (d) Five SMD LED demonstrator, (e) Functional circuit on uneven surface. (f) Detail of the 5 SMD LED demonstrator, soft-soldered using silver paste.

4. Conclusion

Copper tracks on biodegradable PCL have been fabricated using a direct photopatterning method. About 50 μm wide lines have been demonstrated by LED patterning, and 47 $\pm$ 11 μm width by DLW, although thinner tracks could be obtained. The Cu thickness is dependent on the plating time. Cu films prepared at the plating times of 8, 9, 10 min exhibited thicknesses of 5.3 μm, 6.3 μm and 7.8 μm respectively, and showed greater adhesion to PCL substrates compared to Cu films prepared at longer plating times. The electrical conductivity of electroless plated Cu showed a proportional correlation with plating time and reached a plateau of around 2×10^7 S m^{-1} after 15 min of plating. DMA shows a 37% loss of performance after 1000 bending cycles. An 8% strain reveals a conductivity loss of 51%. Finally, Cu plated interconnects were demonstrated to be fully functional in electronic circuits powering a 5 SMD LEDs demonstrator. The direct laser written technique has shown to be able to create conductive copper tracks through uneven surfaces. Therefore, this method has been demonstrated to be a suitable selective metallization technique for the fabrication of conductive tracks on biodegradable substrates for electronics application.

Data availability statement

The data that support the findings of this study are available upon reasonable request from the authors.

Acknowledgments

M A and J M H acknowledge the Libyan Embassy in UK for support under the Grant Ref. 13691. A Z and J M H thank the UK EPSRC for support (EP/T013680/1). We wish to acknowledge the support of the Henry Royce Institute for advanced materials through the Researcher Equipment Access Scheme enabling access to XPS facilities at Cambridge (EPSRC, EP/R00661X/1).

ORCID iDs

Mansour Abdulrhman https://orcid.org/0000-0001-5306-5711
Adilet Zhakeyev https://orcid.org/0000-0003-2571-5398
Carmen M Fernández-Posada https://orcid.org/0000-0003-3080-1637

Ferry P W Melchels https://orcid.org/0000-0002-5881-837X
Jose Marques-Hueso https://orcid.org/0000-0002-1807-3369

References

[1] Hartmann F, Baumgartner M and Kaltenbrunner M 2021 Becoming sustainable, the new frontier in soft robotics *Adv. Mater.* **33** 2004413
[2] Feig V R, Tran H and Bao Z 2018 Biodegradable polymeric materials in degradable electronic devices *ACS Cent. Sci.* **4** 337–48
[3] Gao M, Shih -C-C, Pan S-Y, Chueh C-C and Chen W-C 2018 Advances and challenges of green materials for electronics and energy storage applications: from design to end-of-life recovery *J. Mater. Chem.* A **6** 20546–63
[4] Irimia-Vladu M, Głowacki E D, Voss G, Bauer S and Sariciftci N S 2012 Green and biodegradable electronics *Mater. Today* **15** 340–6
[5] Zhu H, Luo W, Ciesielski P N, Fang Z, Zhu J Y, Henriksson G, Himmel M E and Hu L 2016 Wood-derived materials for green electronics, biological devices, and energy applications *Chem. Rev.* **116** 9305–74
[6] Folino A, Karageorgiou A, Calabrò P S and Komilis D 2020 Biodegradation of wasted bioplastics in natural and industrial environments: a review *Sustainability* **12** 1–37
[7] Cenci M P, Scarazzato T, Munchen D D, Dartora P C, Veit H M, Bernardes A M and Dias P R 2022 Eco-friendly electronics—a comprehensive review *Adv. Mater. Technol.* **7** 1–34
[8] Unda K, Mohammadkhah A, Lee K M, Day D E, O'Keefe M J and Kim C S 2017 Sensor substrates based on biodegradable glass materials *Proc. IEEE Sensors* pp 3–5
[9] Haroon U S and Flint J A 2014 Electro-textile based wearable patch antenna on biodegradable poly lactic acid (PLA) plastic substrate for 2.45 GHz, ISM band applications *Proc.—2014 Int. Conf. Emerg. Technol. ICET 2014* pp 158–63
[10] Mattana G, Briand D, Marette A, Vásquez Quintero A and De Rooij N F 2015 Polylactic acid as a biodegradable material for all-solution-processed organic electronic devices *Org. Electron.* **17** 77–86
[11] Lee C J, Chang Y C, Wang L W and Wang Y H 2019 Biodegradable materials for organic field-effect transistors on a paper substrate *IEEE Electron Device Lett.* **40** 236–9
[12] Guna V K, Murugesan G, Basavarajaiah B H, Ilangovan M, Olivera S, Krishna V and Reddy N 2016 Plant-based completely biodegradable printed circuit boards *IEEE Trans. Electron Devices* **63** 4893–8
[13] Henning C, Schmid A, Hecht S, Harre K and Bauer R 2018 Comparison of different bio-based polymers for electronic substrates *Proc Int Spring Seminar on Electronics Technology* (*1–6 May 2018*) (https://doi.org/10.1109/ISSE.2018.8443764)
[14] Henning C, Schmid A, Hecht S, Harre K and Bauer R 2019 Applicability of different bio-based polymers for wiring boards *Period Polytech. Electr. Eng. Comput. Sci.* **63** 1–8
[15] Huang X, Liu Y, Hwang S W, Kang S K, Patnaik D, Cortes J F and Rogers J A 2014 Biodegradable materials for multilayer transient printed circuit boards *Adv. Mater.* **26** 7371–7
[16] Jack H International application published under the patent cooperation treaty (PCT) WO2018234801A1
[17] Llorens E, Armelin E, Del Mar Pérez-Madrigal M, Del Valle L J, Alemán C and Puiggalí J 2013 Nanomembranes and nanofibers from biodegradable conducting polymers *Polymers* **5** 1115–57
[18] Rajeshkumar G *et al* 2021 Environment friendly, renewable and sustainable poly lactic acid (PLA) based natural fiber reinforced composites—a comprehensive review *J. Clean. Prod.* **310** 127483
[19] European Bioplastics 2017 *Eur. Bioplastics* (available at: https://docs.european-bioplastics.org/publications/market_data/2017/Report_Bioplastics_Market_Data_2017.pdf) (Accessed 12 September 2021)
[20] Melchels F P W, Fehr I, Reitz A S, Dunker U, Beagley K W, Dargaville T R and Hutmacher D W 2015 Initial design and physical characterization of a polymeric device for osmosis-driven delayed burst delivery of vaccines *Biotechnol. Bioeng.* **112** 1927–35
[21] Then Y Y, Ibrahim N A and Yunus M Z W 2011 Enhancement of tensile strength and flexibility of polycaprolactone/tapioca starch blends by octadecylamine modified clay *J. Polym. Environ.* **19** 535–9
[22] Woodruff M A and Hutmacher D W 2010 The return of a forgotten polymer—polycaprolactone in the 21st century *Prog. Polym. Sci.* **35** 1217–56
[23] Lyu J S, Lee J-S and Han J 2019 Development of a biodegradable polycaprolactone film incorporated with an antimicrobial agent via an extrusion process *Sci. Rep.* **9** 20236
[24] Varntanian S 2017 *3D Printing of Polycaprolactone Scaffolds* University of Sheffield
[25] Farah S, Anderson D G and Langer R 2016 Physical and mechanical properties of PLA, and their functions in widespread applications—a comprehensive review *Adv. Drug Deliv. Rev.* **107** 367–92
[26] Cao Y and Uhrich K E 2019 Biodegradable and biocompatible polymers for electronic applications: a review *J. Bioact. Compat. Polym.* **34** 3–15
[27] Valerini D, Tammaro L, Vitali R, Guillot G and Rinaldi A 2021 Sputter-deposited Ag nanoparticles on electrospun PCL Scaffolds: morphology, wettability and antibacterial activity *Coatings* **11** 345
[28] Shin I J and Park M S 2018 Direct conductive patterning on 3D printed structure using laser *Phys. Status Solidi* a **215** 1700597
[29] Filonov D, Kolen S, Shmidt A, Shacham-Diamand Y, Boag A and Ginzburg P 2019 Volumetric 3D-printed antennas, manufactured via selective polymer metallization *Phys. Status Solidi* **13** 1800668
[30] Zhang H N, Wang J, Sun F F, Liu D, Wang H Y and Wang F 2014 Study of electroless copper plating on ABS resin surface modified by heterocyclic organosilane self-assembled film *Bull. Mater. Sci.* **37** 71–76
[31] Luo L-M, Lu Z-L, Huang X-M, Tan X-Y, Ding X-Y, Cheng J-G, Zhu L and Wu Y-C 2014 Electroless copper plating on PC engineering plastic with a novel palladium-free surface activation process *Surf. Coat. Technol.* **251** 69–73
[32] Dixit N K, Srivastava R and Narain R 2017 Electroless metallic coating on plastic parts produced by rapid prototyping technique *Mater. Today Proc.* **4** 7643–53
[33] Shacham-Diamand A, Osaka T, Okinaka Y, Sugiyama A and Dubin V 2015 30 years of electroless plating for semiconductor and polymer micro-systems *Microelectron. Eng.* **132** 35–45
[34] Shao Q-S, Bai R-C, Tang Z-Y, Gao Y-F, Sun J-L and Ren M-S 2016 Durable electroless Ni and Ni-P-B plating on aromatic polysulfonamide (PSA) fibers with different performances via chlorine-aided silver activation strategy *Surf. Coat. Technol.* **302** 185–94
[35] Charbonnier M, Romand M and Goepfert Y 2006 Ni direct electroless metallization of polymers by a new palladium-free process *Surf. Coat. Technol.* **200** 5028–36
[36] Moraczewski K, Rytlewski P, Malinowski R, Tracz A and Żenkiewicz M 2015 Influence of DC plasma modification on the selected properties and the geometrical surface structure of polylactide prior to autocatalytic metallization *Mater. Chem. Phys.* **153** 135–44
[37] Moraczewski K, Mróz W, Budner B, Malinowski R and Żenkiewicz M 2016 Laser modification of polylactide surface layer prior autocatalytic metallization *Surf. Coat. Technol.* **304** 68–75

[38] Zhang Y, Hansen H N, De Grave A, Tang P T and Nielsen J S 2011 Selective metallization of polymers using laser induced surface activation (LISA)—characterization and optimization of porous surface topography *Int. J. Adv. Manuf. Technol.* **55** 573–80
[39] Żenkiewicz M, Moraczewski K, Rytlewski P, Stepczyńska M and Jagodziński B 2015 Electroless metallization of polymers *Arch. Mater. Sci. Eng.* **74** 67–76 (available at: www.scopus.com/inward/record.url?eid=2-s2.0-84948983022&partnerID=10&rel=R3.0.0)
[40] Moraczewski K, Malinowski R, Rytlewski P and Zenkiewicz M 2015 Autocatalytic metallization of polylactide *Polim. Polym.* **60** 492–500
[41] Hasan R M M and Luo X 2018 Promising lithography techniques for next-generation logic devices *Nanomanuf. Metrol.* **1** 67–81
[42] Yang J, Cho J H and Yoo M J 2017 Selective metallization on copper aluminate composite via laser direct structuring technology *Composites* B **110** 361–7
[43] Barbucha R, Kocik M, Mizeraczyk J, Kozioł G and Borecki J 2008 Laser direct imaging of tracks on PCB covered with laser photoresist *Bull. Polish Acad. Sci. Tech. Sci.* **56** 17–20 (available at: https://scholar.google.com/scholar_lookup?title=Laser%20Direct%20Imaging%20of%20tracks%20on%20PCB%20covered%20with%20laser%20photoresist&publication_year=2008&author=R.%20Barbucha&author=M.%20Kocik&author=J.%20Mizeraczyk&author=G.%20Kozio%C5%82&author=J.%20Borecki)
[44] Ratautas K, Gedvilas M, Stankevičiene I, Jagminienė A, Norkus E, Pira N L, Sinopoli S and Račiukaitis G 2017 Laser-induced selective metallization of polypropylene doped with multiwall carbon nanotubes *Appl. Surf. Sci.* **412** 319–26
[45] Gedvilas M, Ratautas K, Kacar E, Stankevičienė I, Jagminienė A, Norkus E, Li Pira N and Račiukaitis G 2016 Colour-difference measurement method for evaluation of quality of electrolessly deposited copper on polymer after laser-induced selective activation *Sci. Rep.* **6** 22963
[46] Marques-Hueso J, Jones T D A, Watson D E, Ryspayeva A, Esfahani M N, Shuttleworth M P, Harris R A, Kay R W and Desmulliez M P Y 2018 A rapid photopatterning method for selective plating of 2D and 3D microcircuitry on polyetherimide *Adv. Funct. Mater.* **28** 1704451
[47] Ryspayeva A, Jones T D A, Khan S R, Esfahani M N, Shuttleworth M P, Harris R A, Kay R W, Desmulliez M P Y and Marques-Hueso J 2019 Selective metallization of 3D printable thermoplastic polyurethanes *IEEE Access* **7** 104947–55
[48] Jones T D A, Ryspayeva A, Esfahani M N, Shuttleworth M P, Harris R A, Kay R W, Desmulliez M P Y and Marques-Hueso J 2019 Direct metallisation of polyetherimide substrates by activation with different metals *Surf. Coat. Technol.* **360** 285–96
[49] Paunovic M 2010 Electroless deposition of copper *Modern Electroplating* vol 1 eds M Schlesinger and M Paunovic (Hoboken, NJ: John Wiley & Sons) pp 433–46
[50] Ryspayeva A, Jones T D A, Esfahani M N, Shuttleworth M P, Harris R A, Kay R W, Desmulliez M P Y and Marques-Hueso J 2019 Selective electroless copper deposition by using photolithographic polymer/Ag nanocomposite *IEEE Trans. Electron Devices* **66** 1843–8
[51] Marques-Hueso J, Morton J A S, Wang X, Bertran-Serra E and Desmulliez M P Y 2018 Photolithographic nanoseeding method for selective synthesis of metal-catalysed nanostructures *Nanotechnology* **30** 15302
[52] Naftaly M, Das S, Gallop J, Pan K, Alkhalil F, Kariyapperuma D, Constant S, Ramsdale C and Hao L 2021 Sheet resistance measurements of conductive thin films: a comparison of techniques *Electron* **10** 960
[53] Waremra R S and Betaubun P 2018 Analysis of electrical properties using the four point probe method *The 3rd International Conference on Energy, Environmental and Information System (ICENIS 2018) E3S Web Conf.* vol 73 pp 1–4
[54] Erdal N B, Lando G A, Yadav A, Srivastava R K and Hakkarainen M 2020 Hydrolytic degradation of porous crosslinked poly(ε-caprolactone) synthesized by high internal phase emulsion templating *Polymers* **12** 4–6
[55] Visan A I *et al* 2020 Long-term evaluation of dip-coated PCL-blend-PEG coatings in simulated conditions *Polymers* **12** 717
[56] Zhou L, He H, Li M C, Huang S, Mei C and Wu Q 2018 Grafting polycaprolactone diol onto cellulose nanocrystals via click chemistry: enhancing thermal stability and hydrophobic property *Carbohydr. Polym.* **189** 331–41
[57] Narkis M, Sibony-Chaouat S, Siegmann A, Shkolnik S and Bell J P 1985 Irradiation effects on polycaprolactone *Polymer* **26** 50–54
[58] Kumar V A, Uchida T, Mizuki T, Nakajima Y, Katsube Y, Hanajiri T and Maekawa T 2016 Synthesis of nanoparticles composed of silver and silver chloride for a plasmonic photocatalyst using an extract from a weed Solidago altissima (goldenrod) *Adv. Nat Sci.: Nanosci. Nanotechnol.* **7** 15002
[59] Fan Y, Bao Y, Song Z, Sun Z, Wang D, Han D and Niu L 2018 Controllable synthesis of coloured Ag0/AgCl with spectral analysis for photocatalysis *RSC Adv.* **8** 24812–8
[60] Boukhvalov D W, Zhidkov I S, Kurmaev E Z, Fazio E, Cholakh S O and D'Urso L 2018 Atomic and electronic structures of stable linear carbon chains on Ag-nanoparticles *Carbon* **128** 296–301
[61] Ferraria A M, Carapeto A P and Botelho Do Rego A M 2012 x-ray photoelectron spectroscopy: silver salts revisited *Vacuum* **86** 1988–91
[62] Ryspayeva A, Jones T D A, Esfahani M N, Shuttleworth M P, Harris R A, Kay R W, Desmulliez M P Y and Marques-Hueso J 2019 A rapid technique for the direct metallization of PDMS substrates for flexible and stretchable electronics applications *Microelectron. Eng.* **209** 35–40
[63] Khalili A, Mottaghitalab A, Hasanzadeh M and Mottaghitalab V 2017 Rejection of far infrared radiation from the human body using Cu–Ni–P–Ni nanocomposite electroless plated PET fabric *Int. J. Ind. Chem.* **8** 109–20
[64] Varol T, Güler O, Akçay S B and Aksa H C 2021 The effect of silver coated copper particle content on the properties of novel Cu-Ag alloys prepared by hot pressing method *Powder Technol.* **384** 236–46
[65] Lee K J, Fosser K A and Nuzzo R G 2005 Fabrication of stable metallic patterns embedded in poly (dimethylsiloxane) and model applications in non-planar electronic and lab-on-a-chip device patterning *Adv. Funct. Mater.* **15** 557–66